

Fatigue surface crack growth behavior in flat plate and out-of-plane gusset-welded joints under biaxial cyclic loads with different phases

Morishita, Mizuki

Department of Civil and Structural Engineering, Graduate school of Engineering, Kyushu University

Gotoh, Koji

Department of Marine Systems Engineering, Faculty of Engineering, Kyushu University

Anai, Yosuke

Physical System Research Group, Industrial System Engineering, Department National Maritime Research Institute

Tsumura, Shuichi

Physical System Research Group, Industrial System Engineering, Department National Maritime Research Institute

他

<https://hdl.handle.net/2324/4751317>

出版情報 : Journal of Marine Science and Technology. 26, pp.655-672, 2020-09-07. Japan Society of Naval Architects and Ocean Engineers (JASNAOE)

バージョン :

権利関係 :



Fatigue surface crack growth behavior in flat plate and out-of-plane gusset-welded joints under biaxial cyclic loads with different phases

Mizuki Morishita¹, Koji Gotoh², Yosuke Anai³, Shuichi Tsumura³, Toshio Niwa⁴

¹Department of Civil and Structural Engineering, Graduate school of Engineering, Kyushu University, 744 Motoooka, Nishi-ku, Fukuoka, 819-0395, Japan.

²Department of Marine Systems Engineering, Faculty of Engineering, Kyushu University, 744 Motoooka, Nishi-ku, Fukuoka, 819-0395, Japan.

³Physical System Research Group, Industrial System Engineering Department National Maritime Research Institute, 6-38-1, Shinkawa, Mitaka-shi, Tokyo, 181-0004, Japan.

⁴Industrial System Engineering Department National Maritime Research Institute, 6-38-1, Shinkawa, Mitaka-shi, Tokyo, 181-0004, Japan.

Abstract

Although many in-service welded built-up structures, which contain many welded joints as fatigue crack initiation sites, are subjected to many types of loading, their structural integrities are evaluated according to design codes based on theoretical and experimental investigations under uniaxial loading conditions. Additionally, most of these codes implement the S-N curves approach. This study highlights the biaxial cyclic loading with different phases. The fracture mechanics approach toward fatigue life evaluation can obtain the fatigue crack growth history. This paper confirms the applicability of previously proposed numerical simulation method for obtaining the fatigue crack propagation histories of a cracked plate subjected to biaxial loads with a phase difference for each loading component. A fracture mechanics approach was used to establish the proposed method. The fatigue surface crack growth behavior of a flat plate and an out-of-plane gusset welded joint under biaxial cyclic loadings with different phases was investigated by extending the applicability of the proposed method to a through thickness crack. Comparisons between the measured crack evolution and the numerical simulation results were carried out to validate our fatigue crack growth simulation for flat plane and welded joints.

Keywords: Fatigue; Biaxial cyclic loading with phase difference; Numerical simulation of fatigue crack growth; RPG stress; Out-of-plane gusset welded joints

1. Introduction

Most in-service welded structures, such as ships and offshore structures, contain many welded joints that can become fatigue crack initiation sites. Additionally, these structures are subjected to many types of loading. However, the structural integrity of most working structures and vehicles is assessed using design codes based on theoretical and experimental investigations under uniaxial loading conditions from a practical viewpoint. The objective of this study was to highlight the biaxial cyclic loading with different phases.

The fatigue strength under biaxial cyclic loading has been investigated based on both the S-N curves approach and the fracture mechanics approach. Studies based on the S-N curves approach [1-3] have only reported S-N curves measured under individual loading conditions. Studies based on the fracture mechanics approach [4-6] have not reached a definite conclusion with regard to the effect of biaxial loading on the fatigue crack growth behavior, owing to contradictory results. Hence, it is very important to establish a quantitative evaluation procedure for fatigue crack growth under biaxial cyclic loading conditions.

Toyosada et al. [7] developed numerical simulation code to evaluate the growth of fatigue cracks with consideration to arbitrary loading histories. To formulate this code, the fatigue crack opening/closing phenomena caused by the existence of the crack wake over the crack surfaces were considered. In this code, the re-tensile plastic zone generating (RPG) stress criterion [7] has been adopted as the fatigue crack propagation law. The RPG stress is defined as the applied remote stress when the re-tensile plastic zone is generated in the vicinity of the crack tip. The improved effective stress intensity factor range is defined by converting the crack opening stress in the fatigue crack propagation law proposed by Elber [8] into RPG stress.

In previous studies, the fracture mechanics approach based on the RPG stress criterion was extended to a biaxial cyclic loading problem, whose loading directions are normal and parallel to the initial crack position. A method for converting the biaxial stress to equivalent uniaxial stress has been proposed and applied to through thickness crack problems [9]. The numerical simulation of fatigue crack propagation under biaxial cyclic loading has been conducted using our developed numerical simulation code for fatigue crack propagation based on the strip yield model [7] under equivalent uniaxial cyclic loading. However, the validity of our method has only been confirmed for through thickness crack problems, and its applicability to surface crack problems has not been verified.

This study investigated the validity of the proposed method [9] for estimating the crack propagation history of surface cracks under biaxial cyclic loading with different phases for two types of test specimens. One specimen type was a flat cruciform-shaped plate containing a surface crack shown in Fig. 1(a). The second specimen type was an out-of-plane gusset welded joint in a cruciform-shaped flat plate shown in Fig. 1(b). The numerical simulation of the surface crack propagation history was performed using the proposed method to convert the equivalent uniaxial loading [9], while the equivalent distributed stress (EDS) method [10] was used to convert the surface crack problem to a through thickness crack problem.

Examples demonstrating the validity of this method under uniaxial cyclic loading have been reported in the literature [11-13].

The objective of this study was to verify the applicability of our numerical approach in estimating the fatigue crack propagation histories of welded joints under biaxial cyclic loads with phase difference.

2. Fatigue surface crack propagation test under biaxial loads with different phases

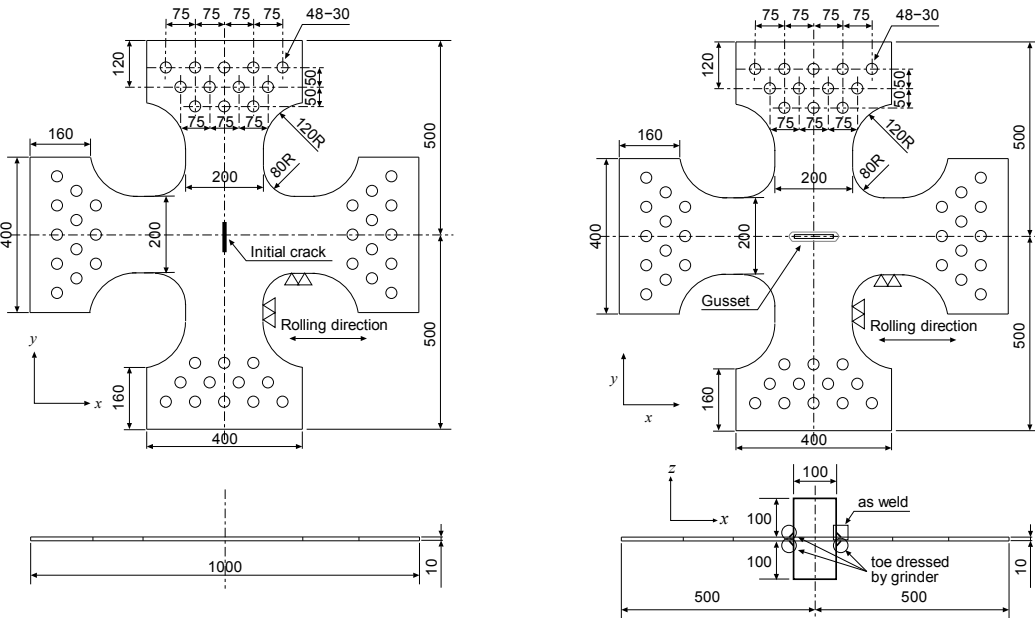
2.1 Specimen configuration and loading condition

The cruciform-shaped surface cracked specimen and out-of-plane gusset-welded joint specimen shown in Fig. 1 were prepared for use in fatigue crack propagation tests under biaxial cyclic loading conditions. The specimen configuration was the same as in Takahashi's in-plane biaxial fatigue test [3]. Specimens S-1 to S-5 had an initial surface crack-like defect in the direction perpendicular to the x-axis, as shown in Fig. 1 (a). Initial defects were formed by electric discharge machining for all the cruciform-shaped surface cracked specimens. The schematic diagram of the initial defect that existed in test specimens S-1 to S-5 and its dimensions are presented in Table 1.

A stiffener (100 mm×100 mm×10 mm) was welded to the cruciform-shaped specimen using corner boxing welding to manufacture an out-of-plane gusset-welded joint specimen. The rolling direction of the stiffener corresponds to that of the cruciform-shaped specimen. The welding condition was one-pass CO₂ semi-automatic arc welding (voltage: 23.4 V, current: 170 A, welding speed: approximately 50 mm/s) using a solid wire (diameter of 0.9 mm, product name MT-50T) such as YGW12 in JIS Z3312 [14]. Generally, a fatigue crack in out-of-plane gusset-welded joint specimens is initiated at the toes of the boxing fillet weld. Owing to the restriction of the fatigue crack initiation site, the three toe regions of the boxing fillet shown in Fig. 1(b) were processed by grinding to relieve the stress concentration. The fatigue cracks in the out-of-plane gusset-welded joint specimens initiated from the as-welded boxing fillet weld toe. Therefore, initial crack wasn't introduced in the joints. All specimens were extracted from the same grade mild steel (ClassNK grade KA [15]). Specimens S-1 to S-4, specimen S-5, specimens G-1 and G-2, and specimens G-3 and G-4 were extracted from a different mild steel plate. The chemical composition and mechanical properties of the tested steel are listed in Table 2 for specimens S-1 to S-4, Table 3 for specimen S-5, Table 4 for specimens G-1 and G-2, and Table 5 for specimens G-3 and G-4. Although different steel plates were applied to fabricate the specimens, the chemical composition and mechanical properties of the applied steels were similar.

Fatigue crack propagation tests were conducted under biaxial cyclic loading conditions using a testing system comprising four independent servo loading actuators that enabled controlled variable loading under different phases (Fig. 2). In this control system, one of the two facing actuators was controlled such that its displacement was the same as the displacement of another facing actuator to hold a central position for the test specimen while monitoring the applied load. The loads applied to each specimen are listed in Table 6. The schematic illustrations of the load waveforms are shown in Figs. 3 and 4. Because G-4 is a re-

in the reference [16].



(b) Out-of-plane gusset-welded joint specimen.

Fig. 1 Configuration of used specimens [3] (unit: mm).

Table 1 Initial crack geometries.

Specimen ID	Initial defect size (mm)		Plate thickness: t (mm)
	Depth: a_0	Length: $2b_0$	
S-1	2.0	4.0	10.0
S-2		20.0	
S-3			
S-4			
S-5			

(Note)
Defect shape

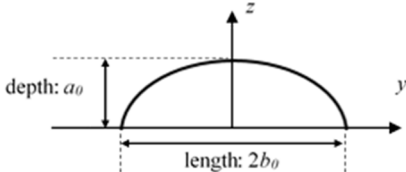


Table 2 Mechanical properties and chemical composition of material applied to specimens S-1 to S-4 (ClassNK grade KA).

Mechanical properties				
Yield stress (MPa)		Tensile strength (MPa)		Elongation (%)
339		456		26
Chemical composition (wt%)				
C	Si	Mn	P	S
0.15	0.14	0.84	0.017	0.003

Table 3 Mechanical properties and chemical composition of material applied to specimen S-5 (ClassNK grade KA).

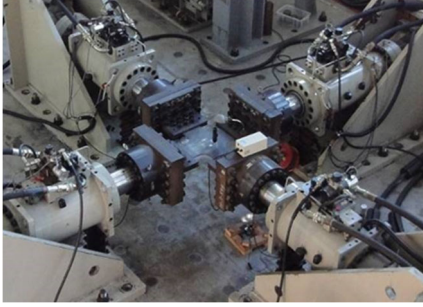
Mechanical properties				
Yield stress (MPa)		Tensile strength (MPa)		Elongation (%)
343		451		26
Chemical composition (wt%)				
C	Si	Mn	P	S
0.12	0.15	0.96	0.021	0.002

Table 4 Mechanical properties and Chemical composition of tested material applied to specimens G-1 and G-2 (ClassNK grade KA).

Mechanical properties				
Yield strength (MPa)		Tensile strength (MPa)		Elongation (%)
298		439		30
Chemical composition (wt%)				
C	Si	Mn	P	S
0.14	0.23	0.86	0.018	0.005

Table 5 Mechanical properties and Chemical composition of tested material applied to specimens G-3 and G-4 (ClassNK grade KA).

Mechanical properties				
Yield strength (MPa)		Tensile strength (MPa)		Elongation (%)
341		461		27
Chemical composition (wt%)				
C	Si	Mn	P	S
0.15	0.14	0.84	0.017	0.003



(a) Flat-cracked specimen.



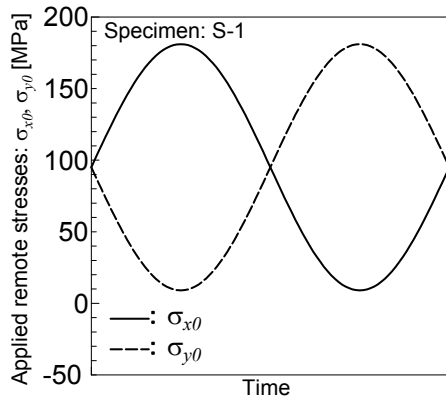
(b) Out-of-plane gusset-welded joint specimen.

Fig. 2 Set-up of fatigue crack propagation test under biaxial loading.

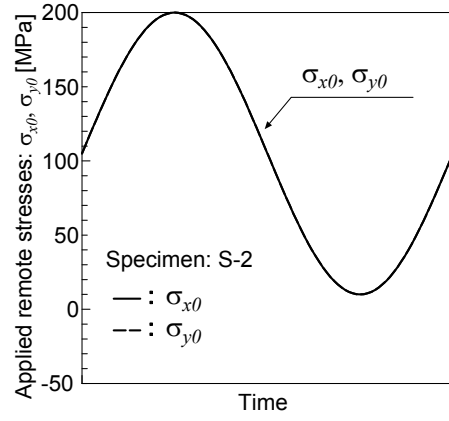
Table 6 Biaxial loading conditions.

Specimen ID	Stress ratio: R	$\Delta\sigma_{x0}$ (MPa)	$\Delta\sigma_{y0}$ (MPa)	Phase difference: Φ (rad)
S-1	0.05	172		π
S-2		190		0
S-3		133		π
S-4		190	95	0
S-5		150	75	π
G-1		110		0
G-2, G-4				π
G-3		130	65	π

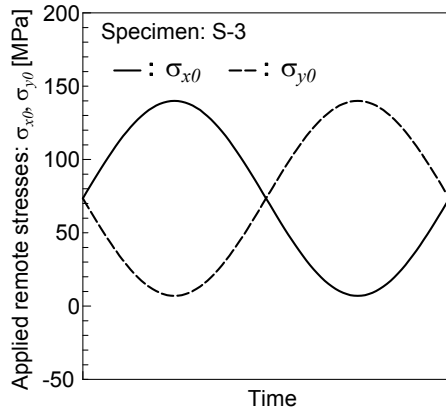
Note: R denotes the applied stress ratio defined by $\sigma_{x0}^{\min}/\sigma_{x0}^{\max}$ or $\sigma_{y0}^{\min}/\sigma_{y0}^{\max}$, $\Delta\sigma_{x0}$ and $\Delta\sigma_{y0}$ are the applied stress ranges of the x and y components, respectively.



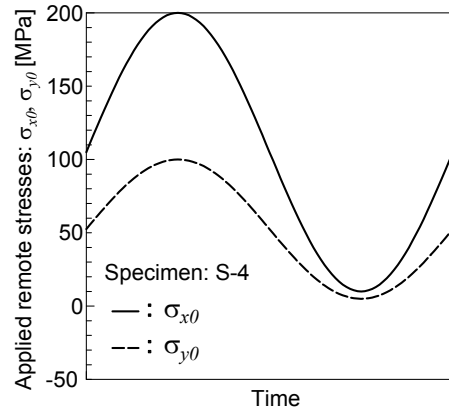
(a) Specimen S-1.



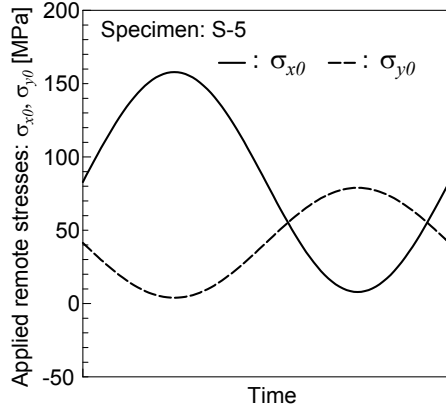
(b) Specimen S-2.



(c) Specimen S-3.



(d) Specimen S-4.



(e) Specimen S-5.

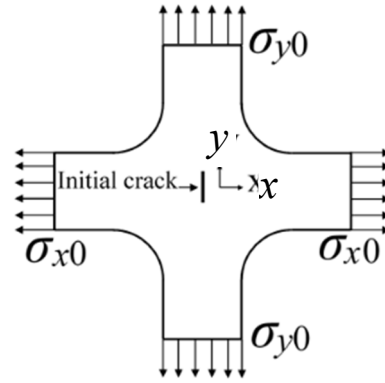


Fig. 3 Applied biaxial loading waveform acting on flat-cracked specimens.

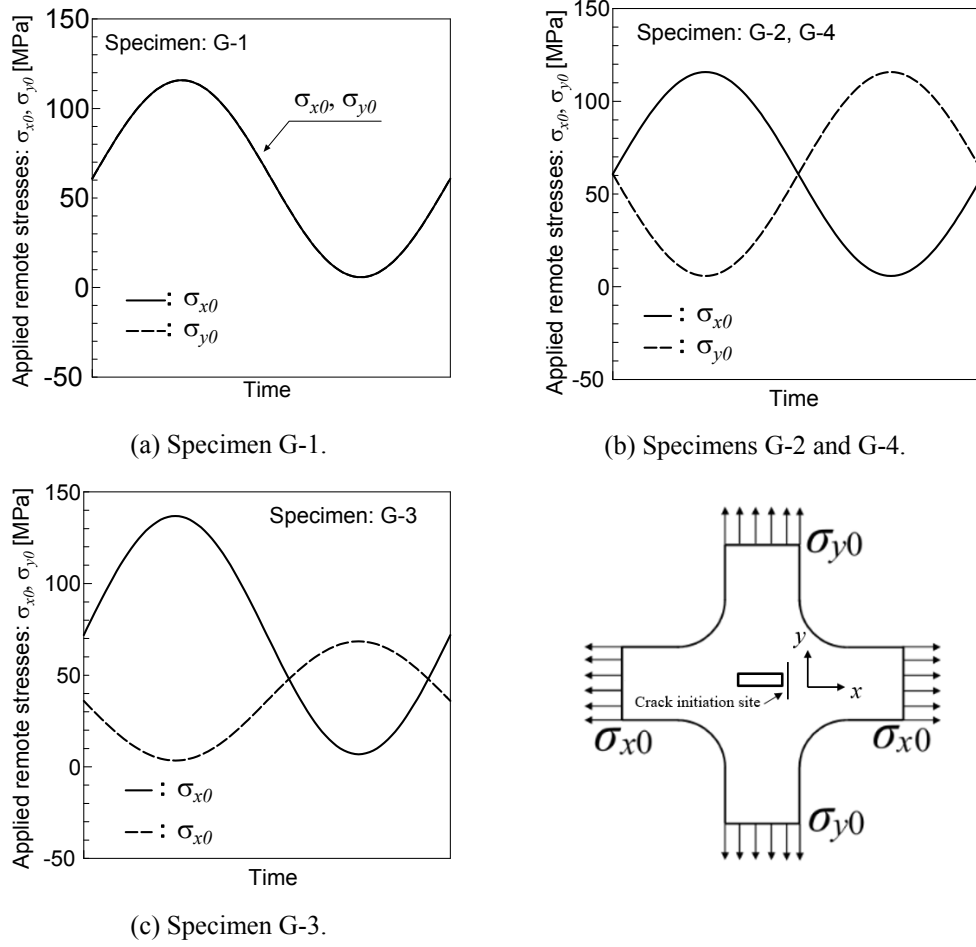


Fig. 4 Applied biaxial loading waveform acting on out-of-plane gusset-welded joint specimens.

2.2 Evolution of surface crack aspect ratio under biaxial loading

The fatigue surface crack propagation histories were measured using the beach mark method. To insert the beach marks, the maximum load was maintained and the minimum load was increased to the average load both in the direction perpendicular and parallel to the surface crack.

The fatigue fracture surfaces of the flat-cracked specimens and out-of-plane gusset-welded joint specimens are shown in Figs. 5 and 6. Figure 7 shows the measured evolution of the aspect ratio a/b during the experiments (a : depth of fatigue surface crack; $2b$: length of fatigue surface crack). In Fig. 7(a), the gray inverted triangle symbols indicate the measurement under uniaxial loading [17]. The solid and dashed curves [18] in Fig. 7(a) were drawn using the empirical formula expressed by Eqs. (1) and (2), which depend on the initial crack shape under the uniaxial loading condition. The solid curve represents equilibrated growth, which is the aspect ratio evolution of a surface crack that initially contains a semi-circular initial defect. The dashed curve represents non-equilibrated growth, which is the aspect ratio evolution of a surface crack that contains an initial semi-elliptical defect. To consider the bending of a test specimen caused by fatigue surface crack propagation, different constants were applied to A and B of Eqs. (1) and (2) before

and after the fatigue surface crack reached half of the plate thickness. As shown in Fig. 7(a), the aspect ratio evolution of a surface crack under biaxial loading was the same as the aspect ratio evolution under uniaxial loading.

For specimens G-1, G-3, and G-4, multiple fatigue cracks occurred close to the as-welded boxing fillet regions. These cracks grew while repeating coalescence and became a large single surface crack. Subsequently, this single surface crack penetrated the base plate, and the fatigue crack continued to propagate as a through thickness crack. In the case of specimen G-2, the evolution process of the multiple surface fatigue cracks was the same as that of specimens G-1, G-3, and G-4. However, in the case of the specimen G-2, it was found that two surface cracks propagated in the different cross sections of the base plate. The step of the fracture surface is shown in Fig. 6(b). Figure 7(b) shows the measured aspect ratio evolutions for each surface crack in the specimens. The aspect ratios were identified by approximating the elliptical shape of a surface crack. The measurement was carried out with regard to the single surface crack after coalescence.

Figures 8 and 9 show the measured fatigue crack growth histories. Accordingly, it was confirmed that the fatigue crack growth rate under biaxial loading was affected by the phase difference of the loading components in Figs. 9(a), (b), and (d). The fatigue crack in specimens G-2 and G-4 with the π phase difference of the biaxial loading component grew faster compared with that of specimen G-1 with zero phase difference. This tendency is related to the phase difference effect being the same as the measurement results for the through thickness cracked cruciform-shaped specimen [9].

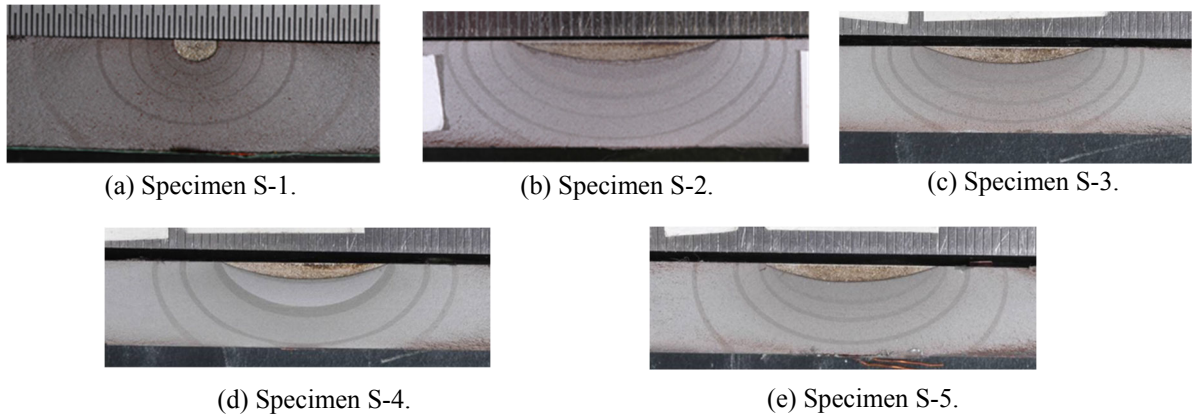


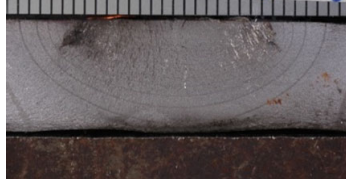
Fig. 5 Observed surface crack shape evolutions for flat-cracked specimens.



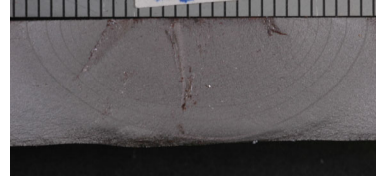
(a) Specimen G-1.



(b) Specimen G-2.

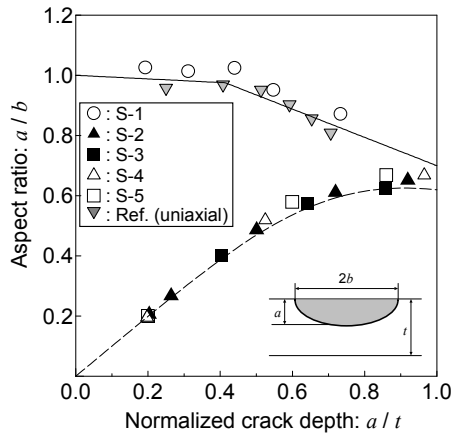


(c) Specimen G-3.

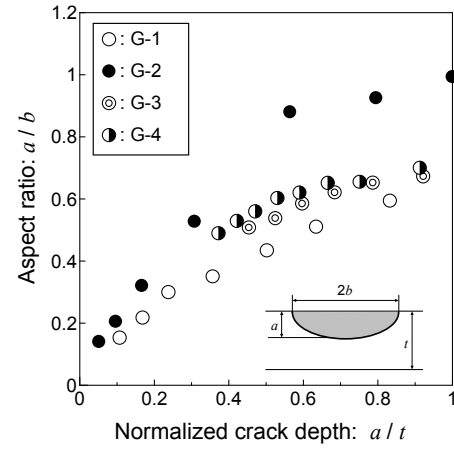


(d) Specimen G-4.

Fig. 6 Observed surface crack shape evolutions for out-of-plane gusset-welded joint specimens.



(a) Flat-cracked specimen.



(b) Out-of-plane gusset-welded joint specimen.

Fig. 7 Evolution of surface crack aspect ratio (a/b) under biaxial loading conditions.

$$a/b = A - B \cdot (a/t) \quad (1)$$

$$(b/a)^n = (b_0/a)^n + \left\{ 1 / (A - B(a/t)) \right\}^n \quad (n = m_p / 2 + 1) \quad (2)$$

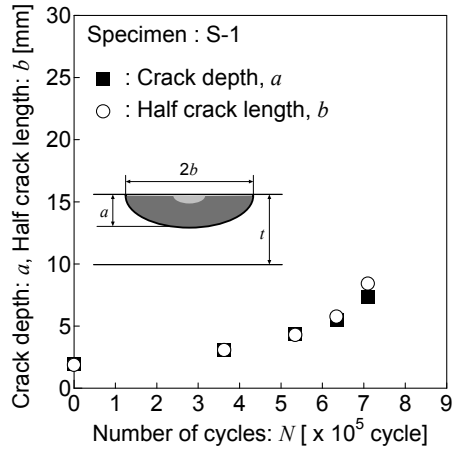
Notes:

$2b_0$: Initial surface crack length

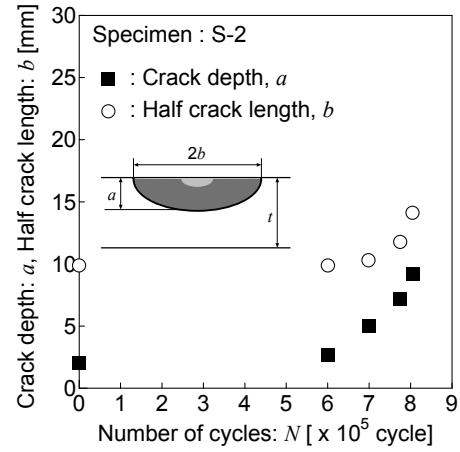
m_p : Constant of Paris' law ($m_p = 3.346$ [19])

A = 0.98 ($0 \leq a/t \leq 0.46$), 1.17 ($0.46 \leq a/t \leq 1.0$)

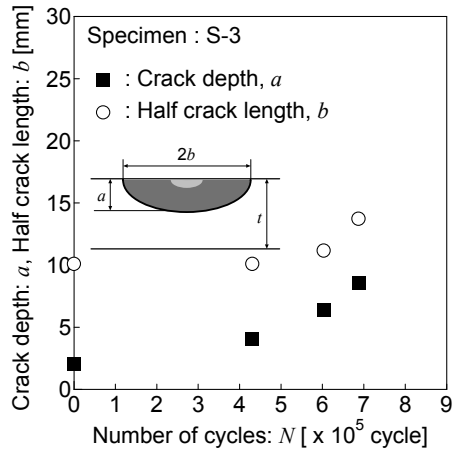
B = 0.06 ($0 \leq a/t \leq 0.46$), 0.47 ($0.46 \leq a/t \leq 1.0$)



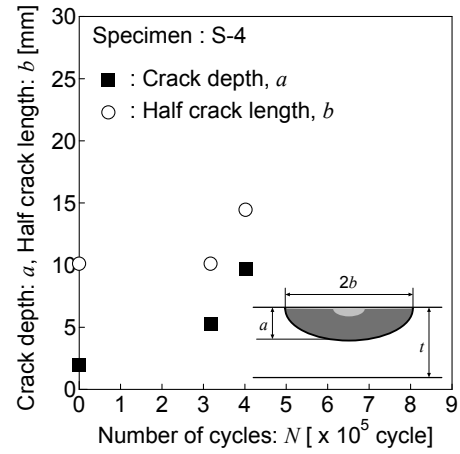
(a) Specimen S-1.



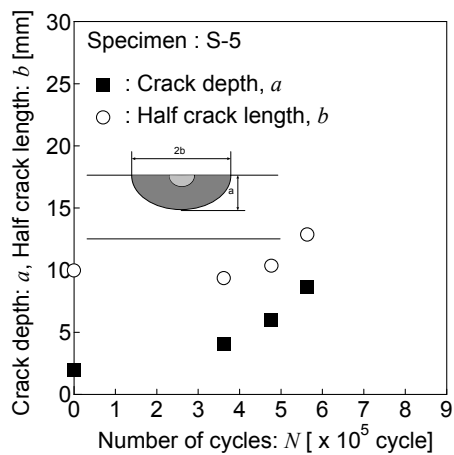
(b) Specimen S-2.



(c) Specimen S-3.



(d) Specimen S-4.



(e) Specimen S-5.

Fig. 8 Measured fatigue crack growth histories of flat-cracked specimens.

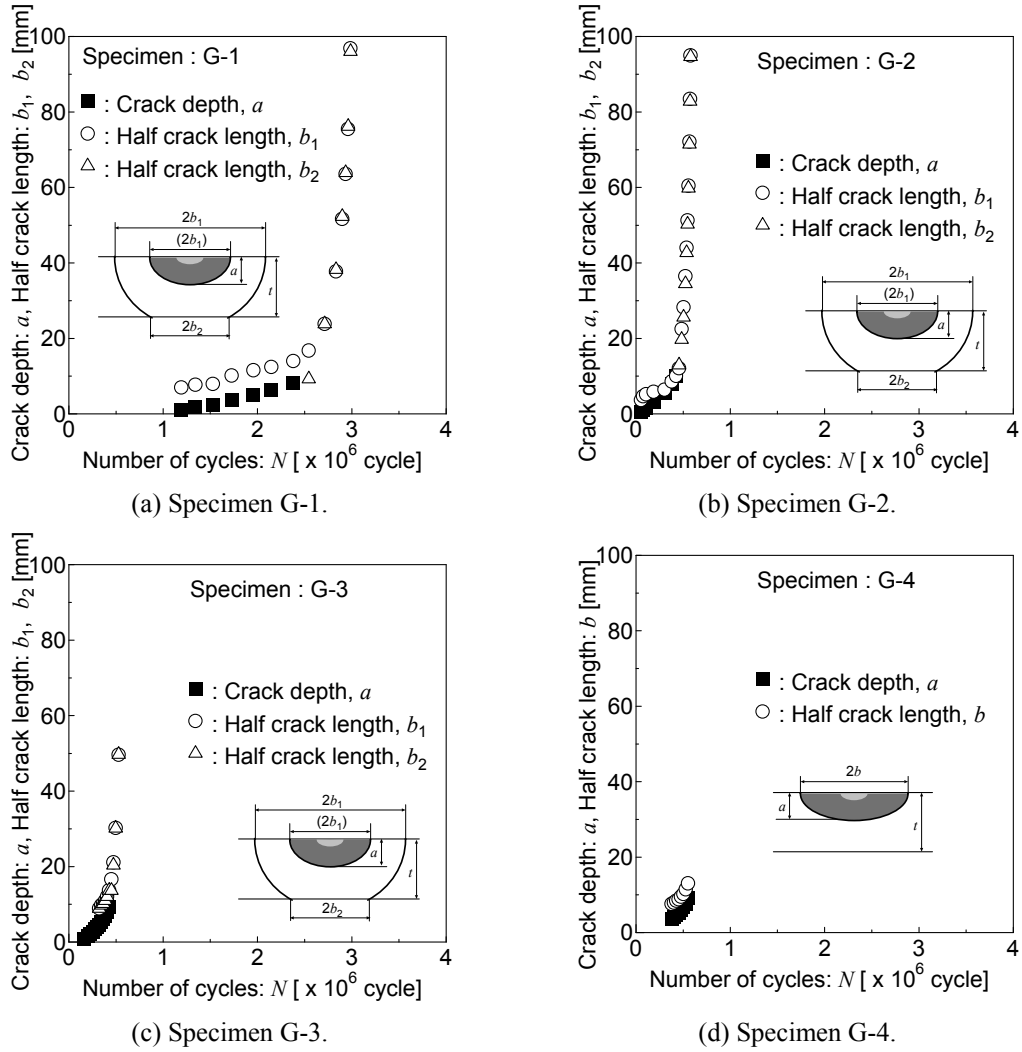


Fig. 9 Measured fatigue crack growth histories of out-of-plane gusset-welded joint specimens.

3. Numerical simulation of fatigue surface crack propagation under biaxial loads with different phases

3.1 Method of converting biaxial stress to equivalent uniaxial stress

The previously proposed method of converting biaxial stress to an equivalent uniaxial stress [9] can obtain the strain at the assumed crack position under a no-crack condition. A simpler and more practical method for obtaining the equivalent uniaxial stress has been previously proposed by the authors [20]. An overview of this simple and a practical conversion method are presented below.

In the case wherein only the stress component is applied in the direction of the crack line, the additional strain induced in the direction perpendicular to the crack propagation direction can be calculated considering Poisson's effect under the plane stress condition expressed in Eq. (3).

$$\varepsilon_x^{\sigma_{y0}} = -(\nu/E)\sigma_{y0} \quad (3)$$

where,

σ_{y0} : applied stress in direction of crack line,

E : Young's modulus,

ν : Poisson's ratio,

$\varepsilon_x^{\sigma_{y0}}$: additional strain in direction perpendicular to crack line.

The stress induced in the direction perpendicular to the crack line by biaxial loading can be obtained as follows:

$$\sigma_x^{\sigma_{y0}} = E\varepsilon_x^{\sigma_{y0}} = -\nu\sigma_{y0} \quad (4)$$

where,

$\sigma_x^{\sigma_{y0}}$: stress induced in direction perpendicular to crack line by $\varepsilon_x^{\sigma_{y0}}$.

The equivalent uniaxial stress can be obtained by adding the induced stress to the applied stress, as follows:

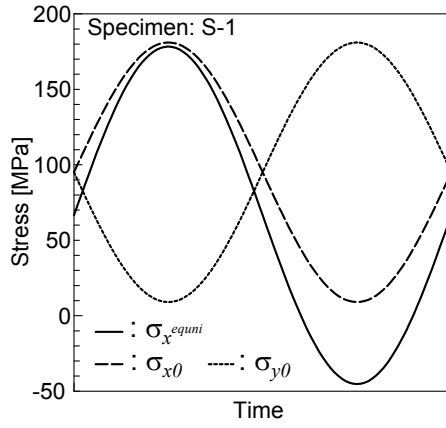
$$\sigma_x^{equi} = \sigma_{x0} - \nu\sigma_{y0} \quad (5)$$

where,

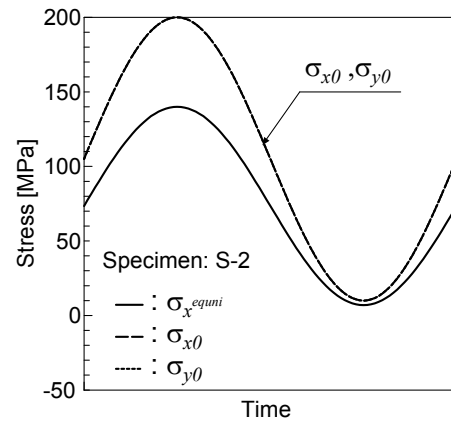
σ_x^{equi} : equivalent uniaxial stress in direction perpendicular to crack line

σ_{x0} : applied stress in direction perpendicular to crack line.

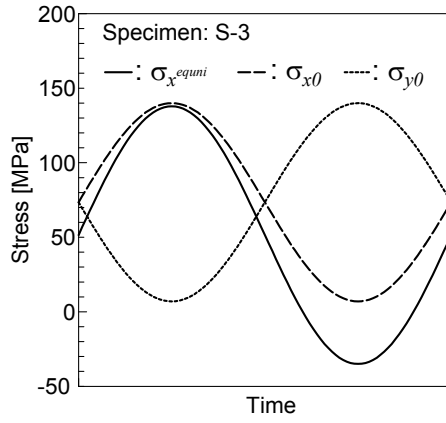
The applied biaxial stress was converted to the equivalent uniaxial stress using Eq. (5). The results are presented in Figs. 10 and 11.



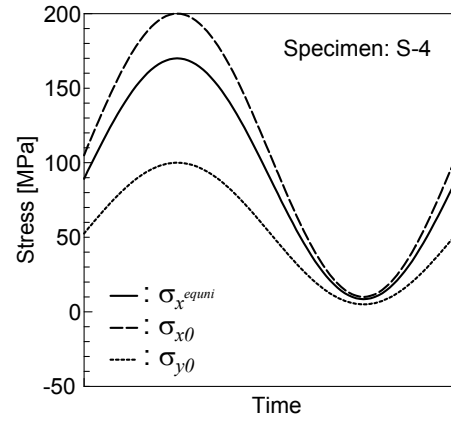
(a) Specimen S-1.



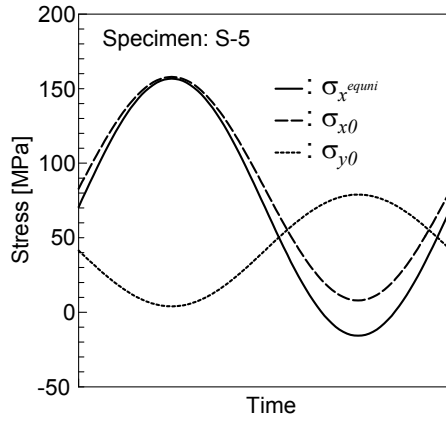
(b) Specimen S-2.



(c) Specimen S-3.



(d) Specimen S-4.



(e) Specimen S-5.

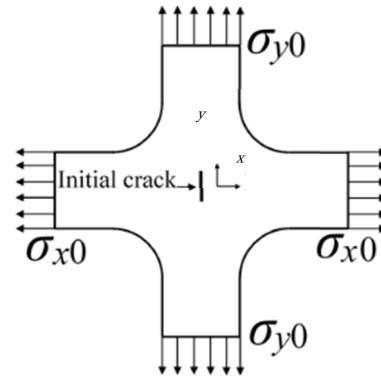


Fig. 10 Applied biaxial stress and equivalent uniaxial stress waveform of flat-cracked specimens.

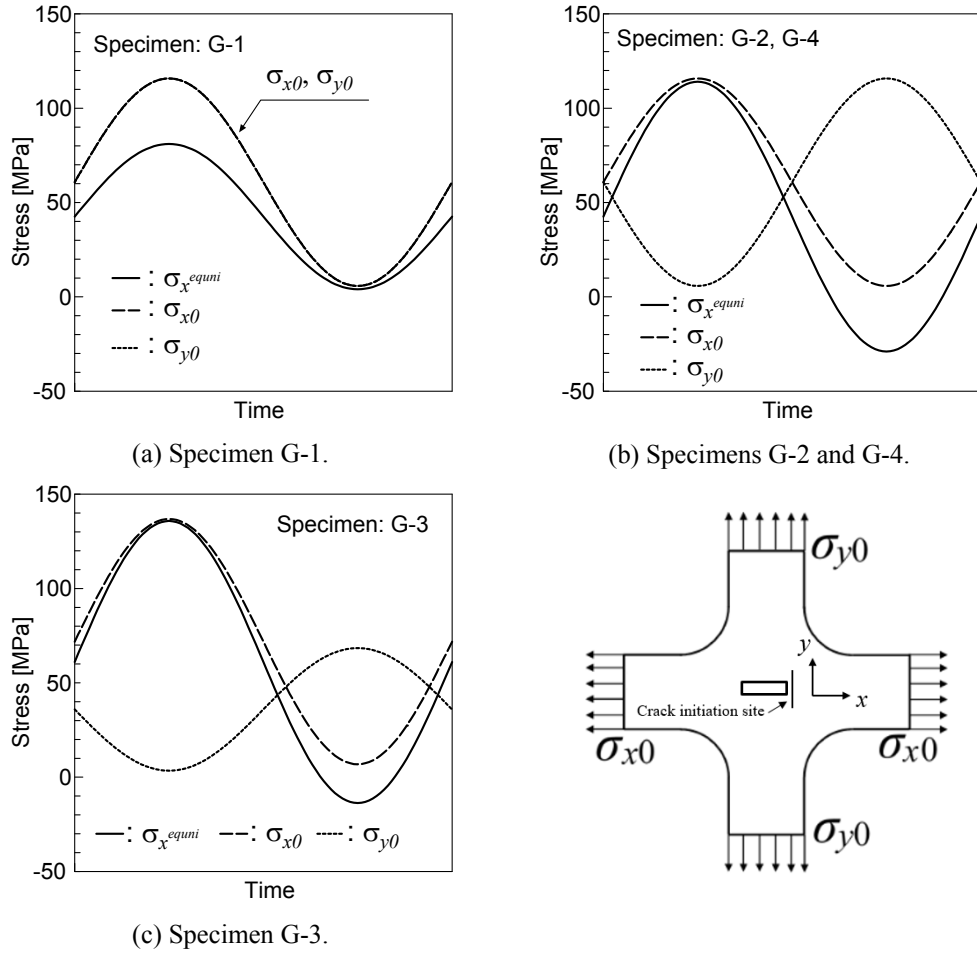


Fig. 11 Applied biaxial stress and equivalent uniaxial stress waveform of out-of-plane gusset-welded joint specimens.

3.2 Numerical simulation of fatigue crack propagation

The numerical simulation of fatigue crack propagation was conducted using our developed code, which models the fatigue crack opening/closing behavior and estimates the relationship between the fatigue crack length and the number of applied loading cycles. The numerical simulation model is based on the strip yield model with a stress intensity factor weight function. The details regarding the theoretical background of this model have been reported in a previous paper [7].

In this numerical simulation, the fatigue crack propagation law based on Paris' fatigue crack propagation law using the RPG stress criterion is expressed as follows:

$$da/dN = C(\Delta K_{RPG})^m \quad (6)$$

where a is the crack length, N denotes the number of cycles, ΔK_{RPG} is the effective stress intensity factor range based on the RPG stress criterion [7], C and m are material constants, and ΔK_{RPG} denotes the period

wherein the re-tensile plastic zone appears at the crack tip in the place of ΔK in Paris' law. The following values [9] were obtained using the same material and specimen geometry, and were applied to the numerical simulation; the units of ΔK_{RPG} and crack length are $\text{MPa m}^{0.5}$ and m, respectively.

$$C = 4.888 \times 10^{-11}, m = 2.824 \quad (7)$$

3.3 Equivalent distributed stress method

Our numerical simulation code for fatigue crack propagation cannot be directly applied to a cruciform-shaped specimen or arbitrary-geometry-shaped specimen with a crack or raked structures, because the explicit expression of the weight function of the stress intensity factor for such joints or structures has not been established yet. Hence, an alternative method is proposed, namely, the equivalent distributed stress (EDS) method [10] for estimating the fatigue crack propagation histories. The flow can be calculated by applying the EDS method as follows:

- (1) Obtain the relationship between the fatigue crack length and the stress intensity factor (K). In a surface crack problem, either the crack depth or the crack length is considered as the representative crack length. In this study, the half-surface crack length (b) was considered as the reference crack length.
- (2) Transform the b - K relationship into EDS as a function of the crack length. The EDS enables the reproduction of the stress field close to the crack tip of planar cracks in an infinitely wide plate with a through thickness crack. The EDS must satisfy the following equation:

$$\frac{2P}{\sqrt{\pi b}} \frac{1}{\sqrt{1-(y/b)^2}} = K \quad (8)$$

$$\int_0^b \frac{2\sigma_{EDS}(y)}{\sqrt{\pi b}} \cdot \frac{1}{\sqrt{1-(y/b)^2}} dy = K_{\text{object}}(b) \quad (9)$$

where,

b : Half crack length,

K : Stress intensity factor at crack length b

P : Concentrated load applied along crack line,

$\sigma_{EDS}(y)$: EDS at crack length y ,

$K_{\text{object}}(b)$: Stress intensity factor at crack length b .

The K value formula Eq. (8) proposed by Tada et al. [21] was adopted in the derivation of Eq. (9).

K in Eq. (8) is stress intensity factor in infinite wide plate which containing a crack with length of

b when concentrated load P is applied along crack line.

- (3) Perform the numerical simulation of fatigue crack growth for an infinitely wide plate with a through thickness crack under the condition of the EDS being distributed along the crack line.

3.4 Stress intensity factor of cruciform-shaped cracked specimens and out-of-plane gusset-welded joint specimens

For flat-cracked specimens, the stress intensity factor at the surface point of the surface crack was calculated using the finite element method along with the J-integral method. The commercial finite element (FE) software MSC Marc 2017 [22] was used to perform these calculations. One-fourth FE models were adopted for all cases. The growth of the fatigue surface crack shape was not affected by the stress biaxiality shown in Fig. 7(a). Therefore, the FE mesh subdivisions for each surface crack in the flat-cracked specimens were modeled according to the empirical formula expressed by Eqs. (1) and (2) [17]. An example of FE mesh subdivision for the flat-cracked specimens is shown in Fig. 12. Fig. 12(a) and (b) represent FE surface crack and through thickness crack subdivision respectively.

The stress intensity factor at the surface point of the surface crack in the welded joint specimens was calculated in the same manner as in the case of flat-cracked specimens. An example of FE mesh subdivision for the out-of-plane gusset-welded joint specimens is shown in Fig. 13, which shows the cross-section of the weld toe in Fig. 13(a). Fig. 13(a) and (b) represent FE surface crack and through thickness crack subdivision respectively. As shown in Fig. 7(b), the slight difference in the evolution of the surface crack's aspect ratio was confirmed even amongst specimens G-1, G-3, and G-4, and is attributed to the difference of the bead shape and welding residual stress distribution. Hence, multiple FE models were prepared according to the evolution of each surface crack's aspect ratio, as shown in Fig. 7(b). FE analysis conditions of surface crack and through thickness crack models are shown in Tables 7 and 8.

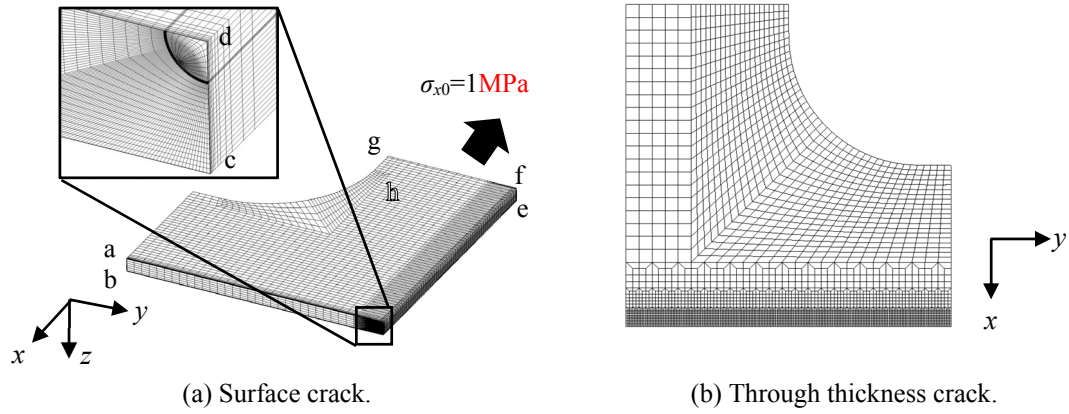


Fig. 12 Example of FE mesh subdivision of flat-cracked specimen.

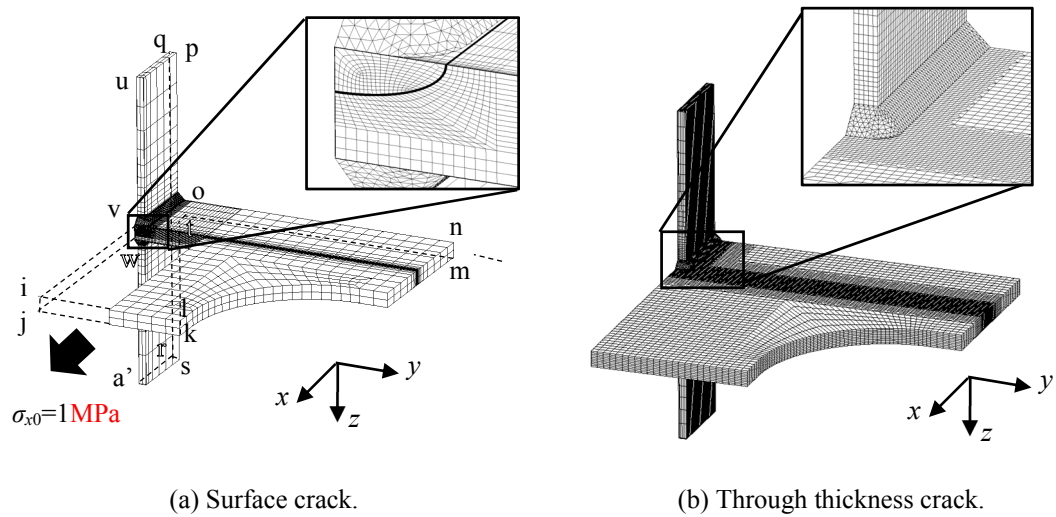


Fig. 13 Example of FE mesh subdivision of out-of-plane gusset-welded joint specimen.

Table 7 FE analysis conditions for surface crack models.

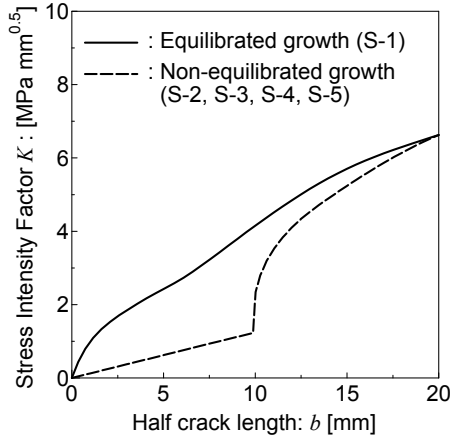
Specimen ID	Interval of crack length [mm]	Min. mesh size [mm]	Element type	No. of elements	No. of nodes
S-1	3	0.02	8-node hexahedral element	203,566 - 224,298	213,691 - 234,855
S-2 – S-5				271,894 - 287,151	283,695 - 299,383
G-1	3	0.1	8-node hexahedral element (Base metal)	76,606 - 170,821	77,323 - 174,394
G-2				77,321 - 152,121	77,950 - 154,672
G-3			4-node tetrahedral element (Weld bead)	89,366 – 104,271	89,806 – 105,481
G-4				89,366 - 104,271	89,806 - 105,481

Table 8 FE analysis conditions for through thickness crack models.

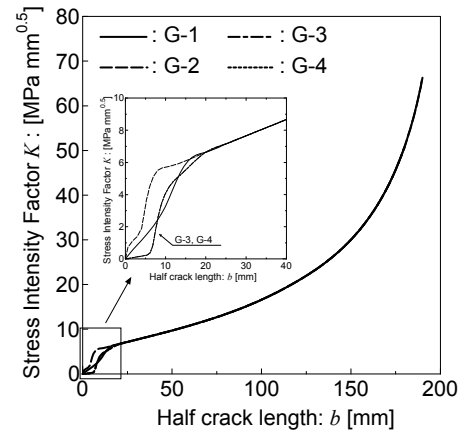
Specimen ID	Interval of crack length [mm]	Min. mesh size [mm]	Element type	No. of elements	No. of nodes
S-1 – S-5	5	1	4-node quadrilateral element	3,925	4,098
G-1 – G-5	5	1	8-node hexahedral element (Base metal) 4-node tetrahedral element (Weld bead)	108,950	114,698

Figure 14 shows the calculation results interpolated by the spline curve. The value of each stress intensity factor was calculated under the unit stress and uniaxial loading condition, whose loading direction was perpendicular to the crack surface as shown in Figs. 12 and 13. Boundary conditions of symmetry planes abcd, dcfe in Fig.12(a) and symmetry planes mnopqrst, ijwa'rquv in Fig.13(a) were decided by considering symmetric condition (For example, translational displacement x of nodes on symmetry plane abcd were fixed). Unit stress was applied on surface efgh in Fig.12(a) and surface ijkl in Fig.13(a). In Fig. 14(a), the solid and dashed curves indicate the stress intensity factor for the equilibrated and non-equilibrated growth, respectively.

The solid, dashed, dashed-dotted, and dotted curves in Fig. 14(b) indicate the stress intensity factor for specimens G-1, G-2, G-3, and G-4, respectively. The units of the applied stress, stress intensity factor (K), and crack length (b) are MPa, $\text{MPa mm}^{0.5}$, and mm, respectively. The EDS calculated from Fig. 14 is shown in Fig. 15.

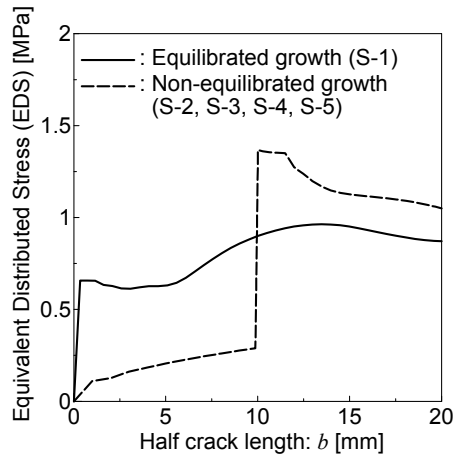


(a) Flat-cracked specimen.

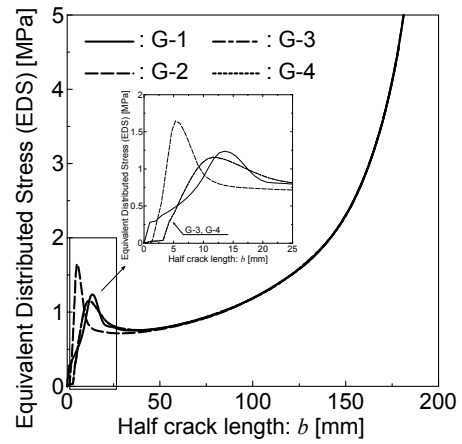


(b) Out-of-plane gusset-welded joint specimen.

Fig. 14 Stress intensity factors as function of crack length under uniform tensile stress.



(a) Flat-cracked specimen



(b) Out-of-plane gusset-welded joint specimen

Fig. 15 Equivalent distributed stresses by unit external loading.

3.5 Stress intensity factor and equivalent distributed stress caused by welding residual stress

The calculation of the stress intensity factor caused by the welding residual stress was performed in two steps: (1) Calculation of welding residual stress in the direction perpendicular to the crack surface using thermo-elastic-plastic analysis; (2) J-integral method under the residual stress field.

The FE mesh subdivision for elastic-plastic analysis was the same as in Fig. 13(b). The welding heat input was set to 67.5 J/mm by considering the welding conditions during the test specimen production. Temperature-dependent material properties are shown in Fig. 16. These properties were decided by referencing documents [23, 24]. The density (ρ) was constant value (7.8×10^{-6} kg/mm³) regardless of temperature. First, the heat input was provided to the face weld bead. The same heat input was provided back to the weld bead after sufficient air-cooling had been allowed for the face weld bead. The residual stress was calculated after air-cooling had been allowed at the back of the weld bead. The obtained residual

stress distribution is shown in Fig. 17, where the vertical axis represents the residual stress in the direction perpendicular to the crack surface (x direction). In Fig. 17, the horizontal axis represents the crack length direction from the center of specimen (y). Calculation result of weld residual stress by inherent stress method [25] for the out-of-plane gusset-welded joint is also shown in Fig. 17. Estimated results by FE analysis agrees with the calculation result by inherent stress method. Hence, estimated result by FE analysis considered appropriate. Coordinates x and z in Fig. 17 represent distance from weld toe and front surface respectively. The J-integral value was calculated by applying the obtained weld residual stress on the crack surface, and the stress intensity factor was converted from the J-integral value. In the case of through thickness crack, the same FE model was used for calculating stress intensity factor and weld residual stress. In the case of surface crack, calculated weld residual stress was applied to FE mesh subdivision of surface crack by interpolating stress distribution.

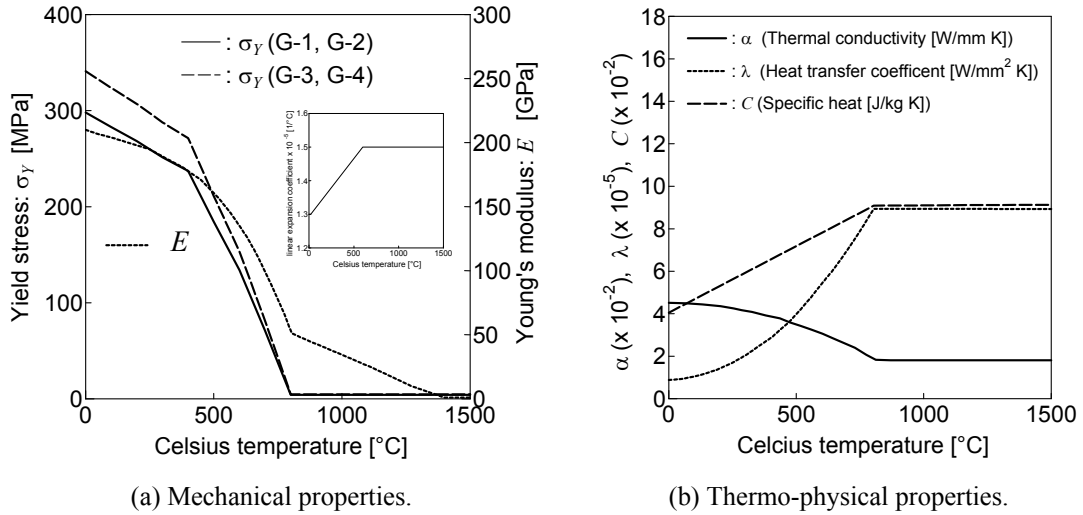


Fig. 16 Temperature-dependent material properties.

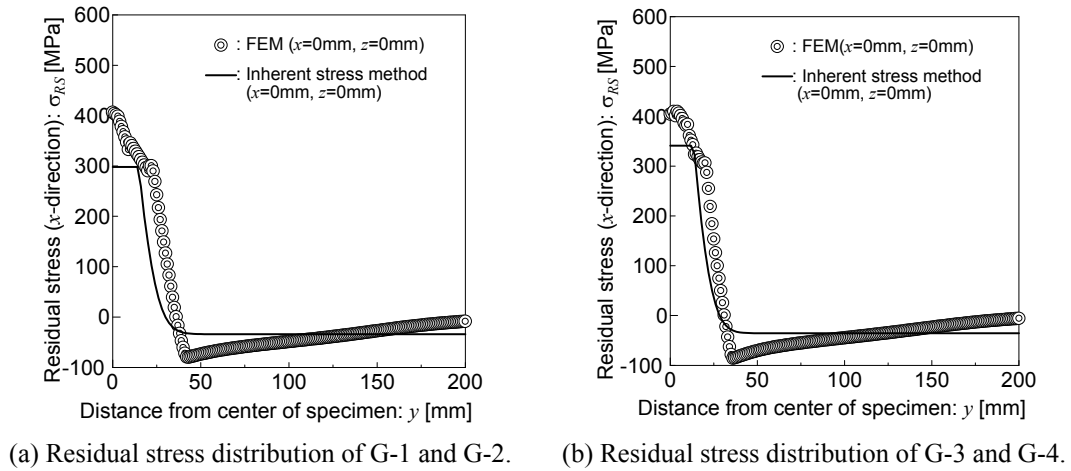


Fig. 17 Residual stress distributions close to fatigue crack initiation site.

Figure 18 shows the stress intensity factor by the residual stress based on the elasto-plastic FE analysis. Figure 19 shows the equivalent distributed stress by the welding residual stress calculated from the stress intensity factor shown in Fig. 18.

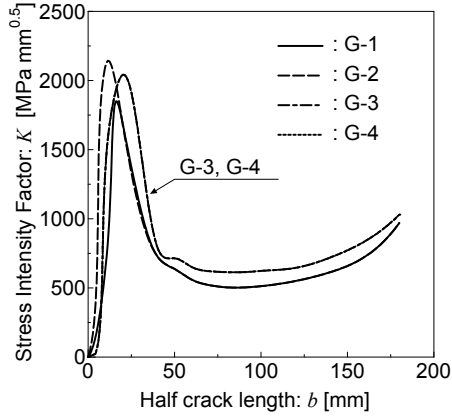


Fig. 18 Relationship between half crack length and stress intensity factor by residual stress based on elasto-plastic FE analysis.

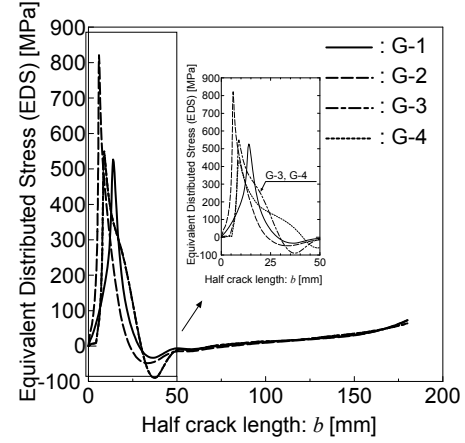


Fig. 19 Equivalent distributed stresses by weld residual stress.

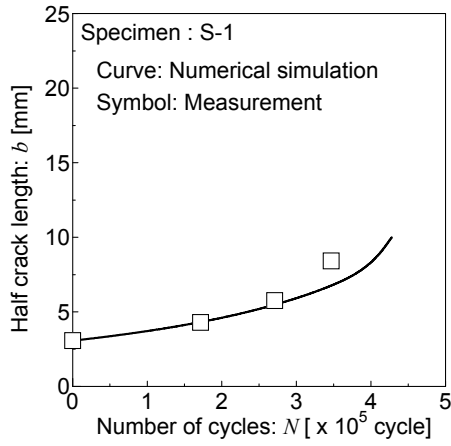
3.6 Fatigue crack propagation analysis

Figures 20 and 21 show the comparison between the fatigue crack propagation histories of the flat-cracked specimens and out-of-gusset-welded joint specimens as obtained by numerical simulation and measurement, respectively. The smallest observed beach mark was considered as the initial crack for specimens S-1 to S-4. The second smallest observed beach mark was considered as the initial crack for specimen S-5, because the fatigue crack length of the smallest beach mark of specimen S-5 did not reach the crack length of the initial defect. After the multiple small fatigue surface cracks at the weld toe became a single large surface crack, the smallest beach mark was considered as the initial crack for specimens G-1 to G-4.

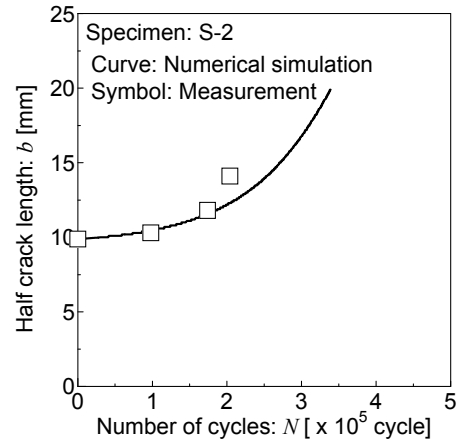
Hence, it is concluded that the proposed numerical simulation method [9-13] can provide a fair, or at least safe, side estimation result. There are various factors that could cause difference between estimation and experimental result, including the followings. Experimental result of S-3 would be caused by thermal influence of electric discharged machining on initial crack tip. Difference between estimation and experimental result of G-3 would be caused by estimation error of WRS as a consequence of application of instantaneous source to calculation of WRS in this paper.

Additionally, from Figs. 21(a), (b), and (d), it can be confirmed that the fatigue life strongly affected the phase difference of biaxial loading. In the case of zero phase difference, the maximum value of σ_{x0} in Fig. 11(a) decreased by the stress in the direction parallel to the crack surface. In the case of π phase difference, the minimum value of σ_{x0} in Fig. 11(b) decreased by the stress in the direction parallel to the crack surface.

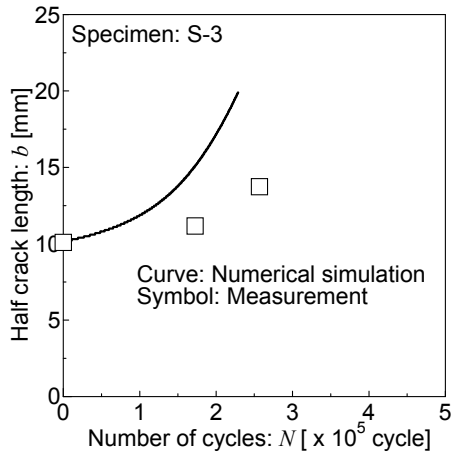
Consequently, the stress amplitude decreased when the phase difference was zero and increased when the phase difference was π , as shown in Fig. 22. This concept, whereby the fatigue life under biaxial cyclic loading is determined by the stress amplitude of the equivalent uniaxial stress, agrees with the test results obtained by a previous study [3].



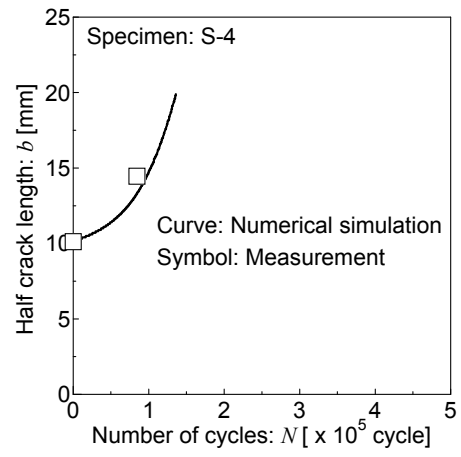
(a) Specimen S-1.



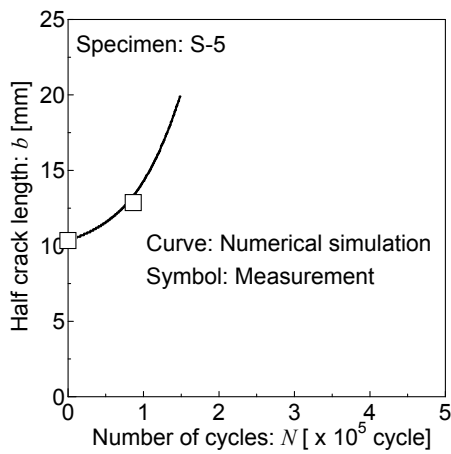
(b) Specimen S-2.



(c) Specimen S-3.

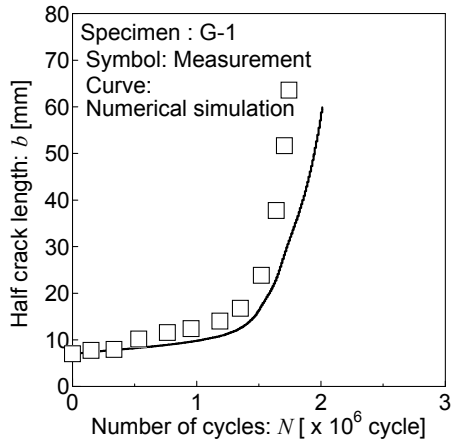


(d) Specimen S-4.

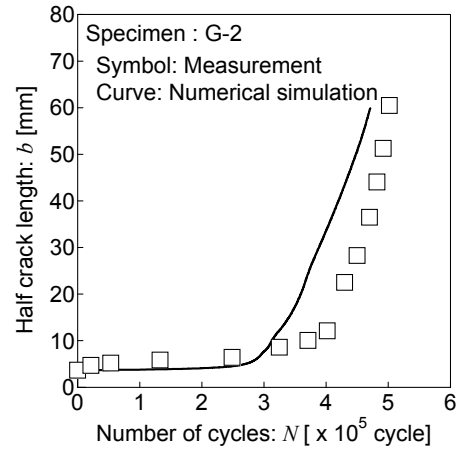


(e) Specimen S-5.

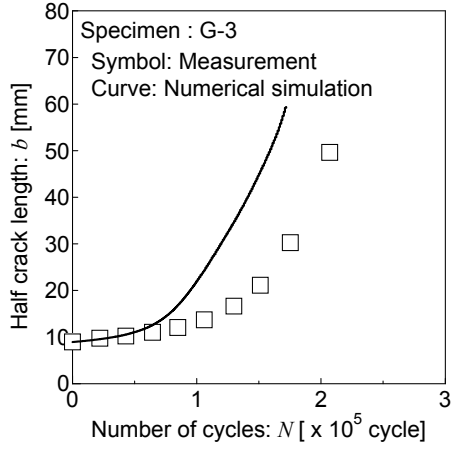
Fig. 20 Numerical simulation results for surface fatigue crack growth of flat-cracked specimens under biaxial loads with phase difference.



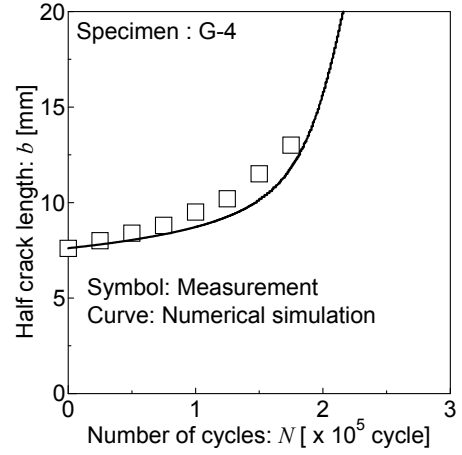
(a) Specimen G-1.



(b) Specimen G-2.



(c) Specimen G-3.



(d) Specimen G-4.

Fig. 21 Numerical simulation results for surface fatigue crack growth of out-of-plane gusset-welded joint specimens under biaxial loads with phase difference.

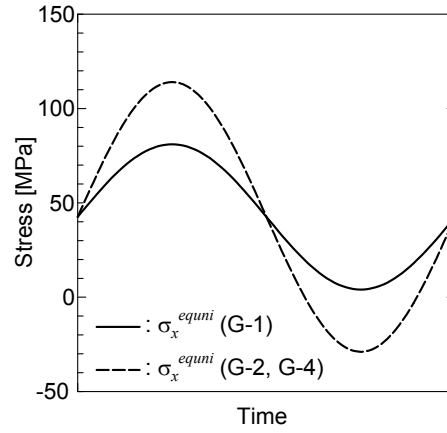


Fig. 22 Effect of phase difference on stress histories.

4. Conclusions

Fatigue surface crack propagation tests were conducted using cruciform-shaped flat-cracked specimens containing initial surface cracks, and out-of-plane gusset-welded joints with a cruciform-shaped flat base plate under biaxial loading and different phase conditions. The results revealed that the aspect ratio evolution of a surface crack under biaxial loading is the same as that under uniaxial loading.

Subsequently, fatigue crack propagation analysis was carried out using a method for converting the biaxial stress to equivalent uniaxial stress, and the previously proposed EDS method [9-13]. This approach was validated for all cases through a comparison between the estimated and measured fatigue crack propagation histories.

In the fatigue surface crack propagation tests using out-of-plane gusset-welded joint specimens, the growth of the fatigue surface crack shape for specimens G-1, G-3, and G-4 was clearly different from that of specimen G-2. The causes for this phenomenon are as follows:

- The weld residual stress distribution difference along the crack surface of each test specimen, which was caused by the heat input difference of manual welding.
- The process wherein multiple fatigue cracks occurring close to the as-welded boxing fillet weld regions grow while repeating coalescence with anti-plane cracks and become a large single fatigue crack with level difference.

Fatigue crack propagation analysis was carried out using the same analysis method as for the flat-cracked specimens. The method was also validated for all out-of-plane gusset-welded joint specimen cases.

The scope of future work is outlined as follows:

- Verify the effect of weld residual stress on the aspect ratio evolution of a surface crack at a welded

joint.

- Verify the proposed method [9-13] for the case wherein each stress wave component with a direction perpendicular and horizontal to the crack surface is a superimposed stress wave containing multiple frequency components.
- Investigate the stress biaxiality effect on the fatigue crack growth inclined with respect to the loading axis.
- Investigate the general multiaxial fatigue problem containing an out-of-plane directional load.

Acknowledgments

This study was funded by a Grant-in-Aid for Scientific Research (A) (No. 26249136) from the Japan Society for the Promotion of Science. The authors would like to express their appreciation to JFE Steel Corporation for supplying the steel plates for the specimens. We thank Edanz Group (<https://en-author-services.edanzgroup.com/>) for editing a draft of this manuscript.

References

- [1] Brown MW, Miller KJ. Mode I fatigue crack growth under biaxial stress at room and elevated temperature. *ASTM STP* 1985;853:135-152.
- [2] Sonsino CM. Multiaxial fatigue of welded joints under in-phase and out-of-phase local strains and stresses. *Int. J. Fatigue* 1995;17:55-70.
- [3] Takahashi I, Ushijima M, Takada A, Akiyama, S, Maenaka, H. Fatigue behavior of a box-welded joint under biaxial cyclic loads. *Fatigue Eng. Mat. Struc* 1999;22:10:869-877.
- [4] Hoshide T, Tanaka K, Yamada A. Stress-ratio effect of fatigue crack propagation in a biaxial stress field. *Fatigue Eng. Mater* 1981;4:355-366.
- [5] Yuuki R, Kitagawa H, Tohgo K, Tanabe M. Effect of bi-axial stress on fatigue crack growth. *Mat. Sci. Research* 1984;33:1271-1277. (In Japanese).
- [6] Yuuki R, Akita K, Kishi N. Effect of biaxial stress condition and its change on fatigue crack growth properties. *Mat. Sci* 1988;37:1084-1089.
- [7] Toyosada M, Gotoh K, Niwa T. Fatigue crack propagation for a through thickness crack. *Int. J. Fatigue* 2004;26:983-992.
- [8] Elber W. The significance of fatigue crack closure. *ASTM STP* 486, 1971:230-242.
- [9] Gotoh K, Niwa T, Anai Y. Numerical simulation of fatigue crack propagation under biaxial tensile loadings with phase differences. *Mar Struct.* 2015; 42:53-70.
- [10] Toyosada M, Gotoh K, Niwa T. Fatigue life assessment for welded structures without initial defects. *Int. J. Fatigue* 2004; 26:993-1002.
- [11] Nagata Y, Gotoh K, Toyosada M. Numerical simulations of fatigue crack initiation and propagation based on re-tensile plastic zone generating (RPG) load criterion for in-plane gusset welded joints. *J.*

Marine Sci. Tech. 2009;14:104-114.

- [12] Gotoh K, Murakami K, Noda Y. Fatigue crack growth behaviour of A5083 series aluminum alloys and their welded joints. JMST, 2011;16:343-353.
- [13] Gotoh K, Takuno M, Okada K, Kusuba S. Numerical simulation of fatigue crack growth of a welded structural component under block program fatigue test. Proceedings of OMAE 2014, OMAE2014-23413.
- [14] Japanese Industrial standards JIS Z 3312. 2009. Solid wires for MAG and MIG welding of mild steel, high strength steel and low temperature service steel. 2009.
- [15] Nippon Kaiji Kyokai (ClassNK). Rules for the survey and construction of steel ships Part K materials. 2019.
- [16] Gotoh K, Niwa T, Anai Y, Fatigue crack growth behavior of an out-of-plane gusset welded joints under biaxial tensile loadings with different phases, Procedia Materials Science 2014;3:1536-1541.
- [17] Anai Y, Niwa T, Gotoh K. Practical formula of the shape evolution of a surface crack under fatigue loading. Proceedings of OMAE 2015, OMAE2015-41978.
- [18] Kawahara M, Kurihara M. A preliminary study on surface crack growth in a combined tensile and bending fatigue process. SNAJ, 1975;137:297-305. (In Japanese).
- [19] Toyosada M, Niwa T, and Sakai J. Physical meaning of ΔK_{RP} and fatigue crack propagation in the residual stress distribution field. Int. J. Fatigue 1997; 19:161-166.
- [20] Gotoh K, Shimizu K, Anai Y, Niwa T. Fatigue crack growth behaviour of out-of-plane gusset welded joints under in-plane biaxial tensile loadings with different phases. JASNAOE 2017;26:157-164. (In Japanese).
- [21] Tada H, Paris PC, Irwin GR. The stress analysis of crack handbook. 3rd Ed. New York: The American Society of Mechanical Engineers; 2000.
- [22] MSC Software. <http://www.mscsoftware.com/ja/product/marc> [accessed 30 October 2019].
- [23] Kim YC, Lee JY, Inose K. The high accurate prediction of welding distortion generated by fillet welding. QJWS 2005; 23.3: 431-435. (In Japanese).
- [24] Sugawara Y, Kataoka K, Ishikawa H. Thermoelastoplastic stress analysis of interruptedly quenched steel. JSME 1987; 53.486: 334-338. (In Japanese).
- [25] Matsuoka K, Yoshii T. Weld residual stress in corner boxing joints. ClassNK technical bulletin 1998;16:1-10.